Open access • Journal Article • DOI:10.1063/1.4927325

Probing the structural and dynamical properties of liquid water with models including non-local electron correlation. — Source link

Mauro Del Ben, Jürg Hutter, Joost VandeVondele

Institutions: University of Zurich, ETH Zurich

Published on: 05 Aug 2015 - Journal of Chemical Physics (AIP Publishing)

Topics: van der Waals force, Density functional theory, Intermolecular force, Molecular dynamics and Electronic correlation

Probing the structural and dynamical properties of liquid water with models including non-local electron correlation

Del Ben, Mauro ; Hutter, Jürg ; VandeVondele, Joost

Abstract: Water is a ubiquitous liquid that displays a wide range of anomalous properties and has a delicate structure that challenges experiment and simulation alike. The various intermolecular interactions that play an important role, such as repulsion, polarization, hydrogen bonding, and van der Waals interactions, are often difficult to reproduce faithfully in atomistic models. Here, electronic structure theories including all these interactions at equal footing, which requires the inclusion of non-local electron correlation, are used to describe structure and dynamics of bulk liquid water. Isobaric-isothermal (NpT) ensemble simulations based on the Random Phase Approximation (RPA) yield excellent density (0.994 g/ml) and fair radial distribution functions, while various other density functional approximations produce scattered results (0.8-1.2 g/ml). Molecular dynamics simulation in the microcanonical (NVE) ensemble based on Møller-Plesset perturbation theory (MP2) yields dynamical properties in the condensed phase, namely, the infrared spectrum and diffusion constant. At the MP2 and RPA levels of theory, ice is correctly predicted to float on water, resolving one of the anomalies as resulting from a delicate balance between van der Waals and hydrogen bonding interactions. For several properties, obtaining quantitative agreement with experiment requires correction for nuclear quantum effects (NQEs), highlighting their importance, for structure, dynamics, and electronic properties. A computed NQE shift of 0.6 eV for the band gap and absorption spectrum illustrates the latter. Giving access to both structure and dynamics of condensed phase systems, non-local electron correlation will increasingly be used to study systems where weak interactions are of paramount importance.

DOI: https://doi.org/10.1063/1.4927325

Probing the structural and dynamical properties of liquid water with models including non-local electron correlation

Mauro Del Ben, Jürg Hutter, and Joost VandeVondele

Citation: The Journal of Chemical Physics **143**, 054506 (2015); doi: 10.1063/1.4927325
View online: http://dx.doi.org/10.1063/1.4927325
View Table of Contents: http://scitation.aip.org/content/aip/journal/jcp/143/5?ver=pdfcov
Published by the AIP Publishing

Probing the structural and dynamical properties of liquid water with models including non-local electron correlation

Mauro Del Ben,[1,a)] Jürg Hutter,[1,b)] and Joost VandeVondele[2,c)]
[1]*Department of Chemistry, University of Zurich, Winterthurerstrasse 190, CH-8057 Zurich, Switzerland*
[2]*Department of Materials, ETH Zurich, Wolfgang-Pauli-Strasse 27, CH-8093 Zurich, Switzerland*

(Received 16 April 2015; accepted 13 July 2015; published online 5 August 2015)

Water is a ubiquitous liquid that displays a wide range of anomalous properties and has a delicate structure that challenges experiment and simulation alike. The various intermolecular interactions that play an important role, such as repulsion, polarization, hydrogen bonding, and van der Waals interactions, are often difficult to reproduce faithfully in atomistic models. Here, electronic structure theories including all these interactions at equal footing, which requires the inclusion of non-local electron correlation, are used to describe structure and dynamics of bulk liquid water. Isobaric-isothermal (NpT) ensemble simulations based on the Random Phase Approximation (RPA) yield excellent density (0.994 g/ml) and fair radial distribution functions, while various other density functional approximations produce scattered results (0.8-1.2 g/ml). Molecular dynamics simulation in the microcanonical (NVE) ensemble based on Møller-Plesset perturbation theory (MP2) yields dynamical properties in the condensed phase, namely, the infrared spectrum and diffusion constant. At the MP2 and RPA levels of theory, ice is correctly predicted to float on water, resolving one of the anomalies as resulting from a delicate balance between van der Waals and hydrogen bonding interactions. For several properties, obtaining quantitative agreement with experiment requires correction for nuclear quantum effects (NQEs), highlighting their importance, for structure, dynamics, and electronic properties. A computed NQE shift of 0.6 eV for the band gap and absorption spectrum illustrates the latter. Giving access to both structure and dynamics of condensed phase systems, non-local electron correlation will increasingly be used to study systems where weak interactions are of paramount importance. © *2015 AIP Publishing LLC.* [http://dx.doi.org/10.1063/1.4927325]

I. INTRODUCTION

Despite the apparent simplicity of the H_2O molecule, bulk liquid water has a rich chemistry and physics. This is commonly illustrated referring to its many anomalous properties, such as the density maximum or the fact that ice floats on water. These macroscopic properties are well characterized experimentally, but resolving the underlying atomistic picture is far more difficult.[1] Indeed, even the structure of the neat liquid is still debated intensely.[2–4] Ultimately, our understanding must go beyond the neat liquid, and the properties of water, as a solvent or reactant, in the bulk, near interfaces or in confinement are of central importance in many fields, such as biology, electrochemistry, catalysis, and earth and climate science.

Theory and simulation can complement the experimental efforts and have a long tradition. For example, liquid water was among the first systems studied when molecular dynamics (MD) based on empirical potentials became available in the 1970s.[5] However, the challenge is significant. Indeed, in the phase diagram, the melting and boiling points are just 100 Kelvin, less than 1 kJ/mol, apart at ambient conditions, implying that small changes in the potential can have dramatic effects on the state of the system. The role of pressure and the flexibility of the hydrogen bonding network can be illustrated by referring to the various stable polymorphs of ice.[6] The fact that various phases are hydrogen disordered highlights the importance of balancing enthalpy and entropy in the description. Not surprisingly, the quest to reproduce all properties of the system is still open, as the properties of the molecule are such that various types of intermolecular interaction have to be described very accurately to resolve the energy scales involved. The electrostatic moments (dipole and higher moments[7]) of the molecule must be faithfully described, the polarizability of the molecule must be captured, the directionality of the hydrogen bond must be included, and dispersion forces must be taken into account. Not surprisingly, several empirical models of various complexities have been developed in order to reproduce the properties of water.[8–22] The most recent models are mostly derived based on high level electronic structure calculation and show excellent agreement with experiment for a variety of properties at low computational cost. However, empirical methods might fail when applied outside their fitting range, and the effort to parameterize the models and refine the employed functional forms cannot be underestimated. This challenge

[a)]delben@chem.uzh.ch
[b)]hutter@chem.uzh.ch
[c)]joost.vandevondele@mat.ethz.ch

rises considerably as soon as solutes come into play, or if more complicated, chemical phenomena, such as autodissociation and reactivity, must be taken into account.

Computing the intermolecular interactions during the entire simulation using electronic structure theory is an alternative to empirical models as complexity increases, since no assumptions on the form of the interactions must be made. However, different electronic structure theories exist that can be employed together with various approximations such as basis sets, and not all theories that can be applied in the gas phase to clusters are available or computationally tractable in the condensed phase. Application of each of these models to bulk liquid water is necessary to gain insight and to benchmark the quality of the level of theory employed, prior to applications involving various chemical species. The pioneering application of electronic structure theory to bulk liquid water was based on density functional theory[23,24] (DFT) using a relatively simple density functional approximation (DFA).[25] The same class of DFA's based on the generalized gradient approximation (GGA) has been employed for most applications (see, e.g., Refs. 2 and 25–41). Yet, GGA DFT has significant short-comings that also influence the quality of the model for bulk liquid water in such a way that contemporary simulation should employ better models. Most notably are the absence of van der Waals (vdW) interactions and a significant self-interaction error. The former leads to a underestimation of the water density,[40,42,43] while the latter leads to an underestimated band gap, with, e.g., implications for redox chemistry[44] and the static dielectric constant.[45] Fortunately, it is possible to go beyond GGA DFT in various ways, and tremendous improvements have been made by including various descriptors of the electronic system to yield models with improved accuracy. In an attempt to classify this progress, Perdew *et al.*[46] employed the metaphor of a "Jacob's ladder" for which each rung of the ladder introduces more descriptors of the electronic system and yields models with improved accuracy. This ladder has currently five rungs which include descriptors (1) the electronic density, (2) its gradient, (3) the kinetic energy density, (4) the occupied molecular orbitals (MOs), typically in a form similar to Hartree-Fock (HF) exchange, and (5) the unoccupied or virtual MO's. GGA DFT belongs to the second rung, while hybrid functionals belong to the forth rung. Increasingly, hybrid functionals are being used for the simulation of liquid water.[47–51] At the fifth rung, the inclusion of the virtual orbitals allows for taking into account non-local, dynamical, electron correlation contributions that contribute to the long-range vdW dispersion interactions. Many of the various functionals on the 5th rung are based on either the random phase approximation (RPA)[52–60] or second-order Møller-Plesset perturbation theory (MP2) in the form of double hybrids (DHs).[61–67] Recently, we presented the first simulations of bulk liquid water based on MP2.[43] It has become possible to combine DFA with two techniques to improve the description of vdW interactions in a way not classified by Perdew. The first technique is based on semi-empirical force-field like contributions, such as the pairwise additive C_6/R^6 term employed by Grimme,[68] while the second introduces an explicit non-local kernel and is referred to as vdW-DF.[69–72] The performance of both these approaches has been extensively tested and the results show a systematic improvement upon the uncorrected GGA or hybrid functionals.[30,34,40,42,51,73,74]

In this work, we assess the performance of various methods, with a focus on functionals from the 5th rung. In particular, the structural and dynamical properties of bulk liquid water have been studied by means of Monte Carlo (MC) and MD simulations. The MC simulations have been performed in the NpT ensemble under ambient pressure and temperature and are focused on the structural properties, while MD has been employed to obtain dynamical observables, namely, the infrared (IR) spectrum and the diffusion constant. Monte Carlo simulations have proven valuable for studying bulk liquid water in earlier work.[41,43,75,76] A significant advantage of the MC scheme is that the sampling of the phase space is solely determined by a total energy based criterion, and that forces and stresses are not explicitly required, simplifying the implementation. The downside is that dynamical properties are not available, and that suitable moves are needed to efficiently explore large portions of the configuration space.[77–81] The reported MC results extend our previous analysis at the MP2 level[43,82] by including several additional DFT methods, including two 5th rung approaches, one based on RPA and one DH. While the tested DH functional shows an anomalous behavior at the RPA level, the calculated density and oxygen-oxygen radial distribution function (RDF) are in excellent agreement with experiments. Additionally, the obtained liquid densities are compared with that of ice I_h calculated at the same level of theory, showing the non-trivial result that, indeed, ice is floating on water. The dynamical (time dependent) properties have been obtained at the MP2 level of theory by MD simulations in the microcanonical (NVE) ensemble. The calculated diffusion constant and infrared spectrum of liquid water are in fair agreement with experiments once the appropriate corrections, in particular nuclear quantum effects (NQEs), are considered. Overall, this supports the view that the MP2 and RPA methods describe the potential energy surface of bulk liquid water accurately and emphasizes the value of treating dispersion interactions at the same level as hydrogen bond interactions.

II. THEORY

The MP2 energy is an effective correction to the Hartree-Fock ground state energy that allows for including dynamical electron correlations. This correction represents the lowest-ranked approximation of a series of systematic improving contributions obtained from Rayleigh-Schrödinger perturbation theory, setting as zero order Hamiltonian the sum of the one electron Fock operators.[61,62] In the canonical orbital form, the MP2 energy E_c^{MP2} takes a compact formulation in terms of MO energies ϵ and four-index two electron repulsion integrals (ERIs) over MO's $(ia|jb)$,

$$E_c^{\mathrm{MP2}} = -\sum_{ij,ab}^{occ,vir} \frac{(ia|jb)[2(ia|jb) - (ib|ja)]}{\epsilon_a + \epsilon_b - \epsilon_i - \epsilon_j}. \quad (1)$$

Here, i, j refer to occupied and a, b to virtual MO's, while the MO ERI's are given by

$$(ia|jb) = \int\int \psi_i(\vec{r}_1)\psi_a(\vec{r}_1)\frac{1}{\vec{r}_{12}}\psi_j(\vec{r}_2)\psi_b(\vec{r}_2)d\vec{r}_1 d\vec{r}_2, \quad (2)$$

where $\psi(\vec{r})$ is a molecular orbital function. Despite its simplicity, the MP2 approach has been, and continue to be, an essential benchmark method for testing new electronic structure theories.[83] Furthermore, a large number of theoretical and algorithmic improvements have been proposed to speed up the computation of the MP2 energy, for example, by lowering the unfavorable scaling with respect to system size (e.g., local-MP2[84–93]), reducing the prefactor in the integral computation (e.g., resolution of identity (RI) approximation[94–97]), and accelerating the convergence with respect to basis set size (e.g., explicitly correlated methods[98]). Here, we describe the RI method, used in this work, as it allows to reduce the required memory and speeds up the integral computation of the MO ERI. Within RI, an auxiliary Gaussian basis $\{\chi_P\}$ is introduced and used to factorize the $(ia|jb)$ ERI's according to

$$\begin{aligned}(ia|jb) \simeq (ia|jb)_{\mathrm{RI}} &= \sum_{RQ}(ia|R)(R|Q)^{-1}(Q|jb) \\ &= \sum_{P} B_P^{ia} B_P^{jb}. \end{aligned} \quad (3)$$

The three center matrix **B**, given by

$$B_P^{ia} = \sum_R (ia|R)L_{PR}^{-1} \quad (4)$$

with $\mathbf{L}^{-1}$ obtained from the Cholesky decomposition of the two center $(R|Q)$ integrals,

$$(R|Q) = \int\int \chi_R(\vec{r}_1)\frac{1}{\vec{r}_{12}}\chi_Q(\vec{r}_2)d\vec{r}_1 d\vec{r}_2 \quad (5)$$

is thus sufficient to compute all the four index ERI's. Therefore, the RI approximation reduces the memory requirements to $O(N^3)$, with N proportional to system size, and, according to Equation (3), the $(ia|jb)_{\mathrm{RI}}$ integrals can be generated from **B** "on-the-fly" using matrix multiplication, greatly improving the efficiency of the overall computation. The application of RI to the evaluation of the MP2 energy has a significant impact in reducing the overall computational cost; nevertheless, the $O(N^5)$ system size scaling of the MP2 method remains unchanged. As a final remark on MP2, the forces acting on the atoms are obtained as derivatives of the total MP2 energy with respect to the atomic coordinates. Due to the non-variational nature of the MP2 energy, the evaluation of the forces is considerably more complex than the counterpart at the standard DFT level. A description of the theory behind the evaluation of the MP2 forces is beyond the scope of this paper, and more details can be found in the literature.[99–103]

A double-hybrid density functional extends a standard hybrid DFT approach by including in the correlation energy a term derived from second-order perturbation theory (PT2) based on the Kohn-Sham (KS) orbitals.[65,66] The general form of the exchange correlation energy of a DH functional can thus be expressed as

$$E_{xc} = (1-a_x)E_x^{\mathrm{DFT}} + a_x E_x^{\mathrm{HF}} + (1-a_c)E_c^{\mathrm{DFT}} + a_c E_c^{\mathrm{PT2}}, \quad (6)$$

where a_x and a_c are mixing parameters. The KS equations are solved using the effective potential associated to the first three terms in Equation (6). The second-order perturbation term E_c^{PT2} is evaluated using a Møller-Plesset-type expression (Eq. (1)) employing the KS orbitals and corresponding eigenvalues as obtained from the converged wavefunction. The double-hybrid density functional considered in this work is named PWPB95-D3.[67] It is based on a reoptimized version of the Perdew-Wang (PW)[104,105] GGA-exchange and Becke95 (B95)[106] meta-GGA-correlation, respectively, for E_x^{DFT} and E_c^{DFT}. The PT2 term includes only the opposite-spin (OS) component of the MP2-type energy[107,108] and the scaling parameters have been obtained by fitting together with a Grimme's D3 type[68] dispersion correction. Introducing the resolution of identity approximation[94–97] to the two electron repulsion integrals over MO's and reformulating the energy denominator in the MP2 expression using the Laplace transformation $1/x = \int_0^\infty e^{-xt}dt$,[109,110] the E_c^{PT2} can be written in a compact form as

$$E_c^{\mathrm{PT2}} = -\int_0^\infty \mathrm{Tr}\left[\mathbf{Q}(t)\,\mathbf{Q}^{\mathbf{T}}(t)\right]dt. \quad (7)$$

Here, $\mathbf{Q}(t)$ is an $N_a \times N_a$ matrix, where N_a is the number of auxiliary basis set functions employed in the RI approximation, and depends on the occupied and virtual MO's and corresponding orbital energies,[108,111]

$$Q_{PR}(t) = \sum_{ia} B_P^{ia} B_R^{ia} e^{t(\epsilon_i - \epsilon_a)}. \quad (8)$$

The total RPA energy[57,58,60,112] is obtained within the exact exchange (EXX) and random phase approximation correlation energies formalism (EXX+RPA). In the framework of EXX+RPA, the total energy $E_{\mathrm{tot}}^{\mathrm{EXX+RPA}}$ is defined as

$$E_{\mathrm{tot}}^{\mathrm{EXX+RPA}} = E_{\mathrm{tot}}^{\mathrm{EXX}} + E_{\mathrm{c}}^{\mathrm{RPA}}, \quad (9)$$

where $E_{\mathrm{tot}}^{\mathrm{EXX}}$ is the total exact exchange energy, sometime referred as HF energy, and $E_{\mathrm{c}}^{\mathrm{RPA}}$ is the RPA correlation energy. These quantities are generally computed employing the orbitals obtained from the converged wavefunction of a given DFT method, commonly at the generalized gradient approximation level, but possibly hybrid functionals or pure Hartree-Fock. For this reason, the EXX and RPA correlation energies are often referred as EXX@DFT and RPA@DFT, or more compactly (EXX+RPA)@DFT, where DFT stands for the specific density functional approximation employed. The EXX@DFT energy is given by

$$E_{\mathrm{tot}}^{\mathrm{EXX}} = \left(E_{\mathrm{tot}}^{\mathrm{DFT}} - E_{\mathrm{xc}}^{\mathrm{DFT}}\right) + E_{\mathrm{x}}^{\mathrm{EXX}}, \quad (10)$$

where the term on the right-hand side is the DFT total energy, the exchange-correlation DFT energy, and the exact exchange energy, respectively. In this work, direct or bare RPA is considered, i.e., exchange like integrals are not included in the computation of RPA@DFT energy. Within this approach, and introducing the RI approximation, $E_{\mathrm{c}}^{\mathrm{RPA}}$ can be expressed in a compact form as a frequency integral

$$E_c^{\mathrm{RPA}} = \frac{1}{2}\int_{-\infty}^{+\infty}\frac{d\omega}{2\pi}\mathrm{Tr}(\log(\mathbf{1}+\mathbf{Q}(\omega)) - \mathbf{Q}(\omega)). \quad (11)$$

Similarly to the E_c^{PT2} case, $\mathbf{Q}(\omega)$ is an $N_a \times N_a$ matrix with elements given by[111,113]

$$Q_{PR}(\omega) = 2\sum_{ia} B_P^{ia} \frac{\epsilon_a - \epsilon_i}{(\epsilon_a - \epsilon_i)^2 + \omega^2} B_R^{ia} \tag{12}$$

with B_P^{ia} defined in Equation (4).

The evaluation of E_c^{PT2} via Equation (7) and E_c^{RPA} via Equation (11) is obtained by carrying out the integration numerically,[113,114] employing a small number of quadrature point N_g independent from the system size (for large gap systems, 6–8 and 30–40 points are sufficient to yield micro-Hartree accuracy, respectively, for E_c^{PT2} and E_c^{RPA}[111,115]). The minimax scheme we have recently implemented for RPA[115] has not yet been employed in the current simulations but allows to reduce to number of points needed for RPA to roughly the number needed for PT2. For each quadrature point, since the RI auxiliary basis set size N_a grows only linearly with the system size, the calculation of $\mathbf{Q}(t)$ and $\mathbf{Q}(\omega)$ has an associated cost that grows $O(N^4)$.[108,113] This scaling behavior represents the asymptotically dominating part for the calculation of the two correlation energies, and, eventually, in the limit of large systems, reflects into the overall computational cost. In this respect, the $O(N^4)$ scaling represents a great improvement when compared to the canonical MP2 and RPA methods, for which the associated costs grow as $O(N^5)$ and $O(O^6)$, respectively. It allows us to evaluate the RPA correlation energy of systems containing up to 512 water molecules.[115]

III. COMPUTATIONAL SETUP

All calculations presented here have been performed with the CP2K program.[116] The KS-DFT method as implemented in the CP2K code makes use of a dual representation for the electronic density and MO's in terms of Gaussian and Plane-Wave (GPW).[117,118] Unless specified otherwise, the Gaussian basis is of correlation consistent triple zeta quality,[119–121] while the PW cutoff is set to the high values of 800 and 1600 Ry, respectively, for EXX+RPA and PWPB95-D3, to ensure convergence at comparatively little cost. To efficiently expand the density and orbitals in plane waves within GPW, core electrons are replaced by pseudopotentials[122] that have been expressly parametrized for the employed functionals. The exact exchange calculations are performed employing a Γ-point implementation making use of a truncated Coulomb operator to avoid divergence of the energy,[48,123] and the truncation radius is set to 6 Å. The evaluation of the correlation energies is obtained within the RI approximation, developed in CP2K in the GPW framework (RI-GPW).[111] The RI auxiliary basis is of the same quality as the primary and specifically fitted for this purpose. In the supplemenatry material,[172] it is shown for the system at hand that the relative error per water molecule introduced by the RI approximation is below 0.002 kJ/mol per molecule. All EXX+RPA calculations reported in this work have been performed employing KS Perdew-Burke-Ernzerhof (PBE)[124] orbitals as input; due to this, in the following, RPA is used as a short hand notation for (EXX+RPA)@PBE, unless when otherwise specified. More details on the computational setups for the other tested methods are reported in the supplementary material.[172] The model system is made of 64 H_2O molecules in a cubic box under periodic boundary conditions (PBCs). The initial configuration has been equilibrated with a ~50 ps NVT-MD run under experimental density at the BLYP-D3[125,126] level. The Monte Carlo simulations have been performed employing the same setup as given in Ref. 43, with thermodynamic constraints set to ambient conditions, that is, $T = 295$ K and $p = 1$ bar. The MC efficiency is improved with the presampling of moves,[77,79] in the actual case, the approximated potential is calculated at the DFT level employing the PBE1W[127] functional, for which the basis and D3 parameters have been specifically refitted in order to reproduce the energetics of the RPA and DH methods as well as possible, and thus to increase acceptance of moves. The equilibrium parameters for ice I_h have been inferred from energy versus volume data fitted with a 3rd order Birch-Murnaghan equation of state. At each fixed volume, the supercell containing 96 H_2O molecule has been relaxed at the PBE0-D3[128] level, RPA, PWPB95-D3 and MP2 energies have been calculated for the obtained geometries. Finally, the correlation energies have been extrapolated to the complete basis set (CBS) limit by employing the two point T-Q formula.[129,130] MD simulations were started from the corresponding equilibrated MC configurations. The MP2 MD simulations used a multiple time step scheme, previously proposed by us in the context of hybrid density functionals.[48] In this case, the fast time step (0.25 fs) corresponds to a PBEW1-D3 simulation, while the slow time step (1.5 fs) is based on MP2, yielding essentially a 3-fold speedup over a standard (0.5 fs) MD run, while retaining accurately the MP2 dynamics. Two independent MP2 MD simulations were performed in the NVE ensemble, both somewhat more than 10 ps in length. The IR absorption cross section $\alpha(\omega)$ was obtained, in the harmonic approximation, from the power spectrum estimation of the time correlation function $M(t) = \langle \vec{\mu}(0) \cdot \vec{\mu}(t) \rangle$ of the cell dipole $\vec{\mu}(t)$,[131]

$$\alpha(\omega) = \frac{2\pi\beta}{3Vc} \frac{\omega^2}{n(\omega)} \int_{-\infty}^{+\infty} M(t) e^{-i\omega t} dt, \tag{13}$$

where $\beta = 1/k_B T$ is the inverse temperature, V is the cell volume, c is the speed of light, and $n(\omega)$ is the refractive index, which has been assumed constant in the current work. In the present case, the dipoles were obtained from the Wannier centers as computed with the PBE0 functional over the frames of the MP2 trajectory. In order to estimate the influence of nuclear quantum effects on the structural properties, a series of molecular dynamics simulations have been performed employing a quantum thermostat (QT) based on the generalized Langevin equation (GLE).[132,133] This elegant scheme accounts in a computationally inexpensive but approximate way for nuclear quantum effects, maintaining a non-equilibrium temperature distribution in a frequency specific way. For these simulations, the temperature is maintained at 300 K at constant volume, and the considered density functional approximation is PBE0-ADMM-D3, where ADMM stands for auxiliary density matrix method.[49] In the ADMM scheme, a smaller auxiliary basis is introduced in order to approximate the non-local HF exchange energy at reduced cost, and the same auxiliary basis as that employed in our previous MC study[43] has been used. The volume is chosen such as to reproduce the calculated

equilibrium density at the PBE0-ADMM-D3 level, that is, 1.023 g/ml.

IV. STRUCTURAL PROPERTIES

First, we discuss structural properties of bulk liquid water, as obtained from Monte Carlo simulations. Reported in Figure 1 is the density fluctuation over the MC trajectory obtained with the RPA and PWPB95-D3 methods. At the RPA level, the density quickly equilibrates, giving an average density of 0.994 g/ml in excellent agreement with the experiment. The root mean square deviations (RMSDs) of the instantaneous density are 0.015 g/ml similarly to that of the MP2 method.[43] As RPA is computationally less demanding than MP2, roughly twice the number of MC cycles has been performed relative to the earlier MP2 work,[43] contributing to the statistical quality of these results. Nevertheless, finite sampling times cannot exclude sudden structural rearrangements on longer time scales. This is observed at the PWPB95-D3 level. Initially, the fluctuations of the instantaneous density seem to equilibrate quite rapidly to a stable average value of 1.002 g/ml with a tighter RMSD of 0.009 g/ml. However, suddenly, at around 24 000 cycles, there is a sharp transition to a high density phase, which is not fully stabilized after the additional 10 000 cycles. Fluctuations between high density (HD) and low density (LD) phases would be expected near a liquid-liquid phase transition, for small samples, but the high computational cost of these simulations does not allow for exploring this in depth. Pragmatically, the results obtained at the PWPB95-D3 level will be analyzed separately for the LD and HD portions of the trajectory, even though statistics for the later case are limited.

Figures 2(b) and 2(c) show the RDF's obtained at the PWPB95-D3 (LD and HD) and RPA level, respectively. For comparison also, the RDF's obtained at the BLYP and PBE0-D3 levels are reported in Figure 2(a). Note that the PBE0-D3 simulation has been performed without the ADMM, i.e., without this approximation for the calculation of the non-local Hartree-Fock exchange energy. For the RPA case, the RDF is in very good agreement with the recent experimental $g_{OO}(r)$ obtained from x-ray diffraction.[134] The height of the first peak is overestimated by around 10%, while the features of the long range part are remarkably well reproduced, being only very

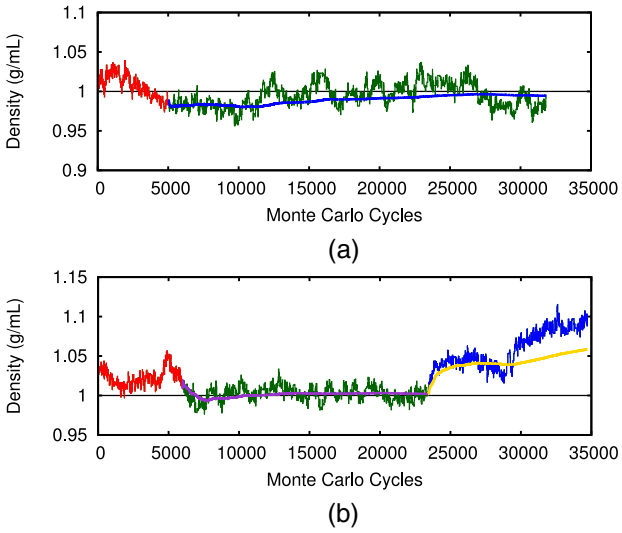

FIG. 1. Fluctuation of the instantaneous density and running average density as a function of Monte Carlo cycles for the NpT simulations ($T = 295$ K and $p = 1$ bar) at the 5th rung. In both cases, the red portion of the plots denotes the cycles considered for equilibration and the horizontal black line represents the experimental density. (a) (EXX+RPA)@PBE, the green parts of the trajectory refer to that used for the calculation of the average properties. (b) PWPB95-D3, in the plot, the two portions highlighted in green and blue refer to the low and high density regimes, respectively.

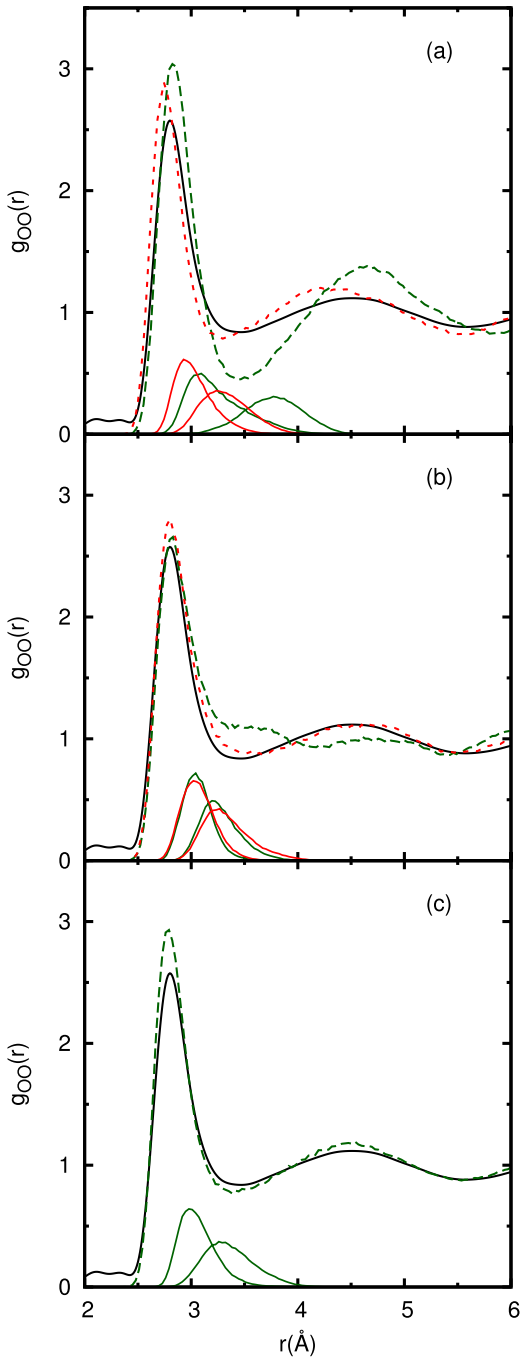

FIG. 2. RDF's for oxygen-oxygen distances from the NpT-MC simulations ($T = 295$ K and $p = 1$ bar). (a) BLYP (green dashed) and PBE0-D3 (red dotted); (b) PWPB95-D3 high density (green dashed) and PWPB95-D3 low density (red dotted); (c) RPA (green dashed). The solid red and green lines give the partial contributions to the total RDF's from the 4th and 5th neighboring water molecules. The solid black line represents the experimental oxygen-oxygen RDF, obtained from x-ray diffraction and taken from Ref. 134.

slightly more structured. The PWPB95-D3 approach matches the experimental shape nicely with the LD $g_{OO}(r)$, but the HD counterpart retains only the first peak and is completely unstructured for the mid and long range parts, suggesting a structural collapse.

In order to gain additional information on the local environment around each water molecule in the liquid, the positions of the 4th and 5th neighboring H_2O are analyzed, as they serve as an indicator for the level of penetration of the second coordination shell into the first. These partial contributions to the total $g_{OO}(r)$ of the forth and fifth neighboring water molecules are reported as solid (green and red) lines in the RDF's of Figure 2. It is a well known result that density functional approximations not including van der Waals interactions give highly structured and significantly less dense (around 10%-20%) liquids.[40–42] This is shown in Figure 2(a) for the BLYP case, but similar shapes are obtained with other semi-local as well as hybrid functionals. The introduction of dispersion forces, either in a semi-empirical way, such as the Grimme's D3 correction, or by including an explicit non-local term in the functional, such as in the van der Waals density functionals,[69,70] improves the liquid description, but in general gives too dense water (5%-10%).[38,40,42,74,135,136] An illustration of the change induced by van der Waals interactions is provided in Figure 2(a), where BLYP and PBE0-D3 RDF's are shown. In particular, the distributions of the 4th and 5th neighboring waters show a clear separation between the first and second coordination shells in the BLYP case, whereas these peaks move closer at the PBE0-D3. The fact that both peaks move also to shorter distances in the later case is probably due to the increased value of the average density (0.797 and 1.053 g/ml for BLYP and PBE0-D3, respectively).

These results match with the models proposed for high/low density liquid (HDL, LDL),[137] for which the latter corresponds to an ice-like tetrahedral structure and the former is associated with a distortion of the H-bonding in the first coordination shell allowing for the intrusion of molecules from the second shell. Even though our calculations do not directly provide support for the actual existence of a HDL/LDL phase coexistence in physical system, it is clear that models might be biased to one or the other phase based on the quality of the model and the approximations made. The LDL is favored by directional strong H-bonding, and the HDL is more favored by isotropic dispersion forces giving a preferred hexagonal arrangement. Indeed, approaches that are missing van der Waals interactions or are over polarized are most likely to lead to LDL, while methods for which dispersion forces are included bias the description to the HDL structure. If the relative strength of H-bonding and van der Waals interactions is not balanced, then the description of the liquid results to be either overstructured with low density (LDL-like) or understructured with high density (HDL-like). The accurate prediction of the water density and structure requires thus accurate balance between these two fundamental interactions. On this basis, it can be argued that the accurate prediction of the water density and structure by RPA and MP2 can be attributed to the fact that these theories provide, for this system, a correct balance between hydrogen-bond and van der Waals interactions. Reaching this balance might be facilitated by the fact that both interactions are obtained from the same level of theory. Note that in general, MP2 and RPA tend to overbind and underbind, respectively, noncovalent complexes as found in the S22 set,[138] which covers a broader range of complexes, including compounds that are aromatic or have double bonds.[60,130,138,139] While these effects are not pronounced for water, it might nevertheless lead to the slightly higher and lower water densities calculated at the MP2 and RPA levels, respectively.

To put these results in context, Table I summarizes the density and structural features of the RDF of liquid water obtained from NpT-MC simulations at different levels of theory, but with consistent choice of simulation parameters. In addition to functionals including orbital correlation (RPA, PWPB95-D3, and MP2), and standard GGA and hybrid functionals (BLYP, PBE, and PBE0), other density functional approximations have been considered such as non-local van der Waals functionals (optB88-vdW[140,141] and rVV10[71]) and meta-GGA functionals (M062X, M06, and M06L belonging to the Minnesota suite[142,143]). In Table I, Δ_ρ represents an estimation of the error in the calculation of the average density ρ. The protocol employed for calculating Δ_ρ is reported in the supplementary material.[172] As shown in the last column of Table I, not all the MC simulations have been run with the same number of cycles. The reasons for this are (a) the significantly different computational costs associated to the different methods (see Table II in the supplementary material[172]) and (b) the different number of cycles required to reach a stable running average density. The simulation with the computationally most demanding methods (e.g., MP2, RPA, and PWPB95-D3) is by necessity shorter. Nevertheless, similar estimated errors for the average density are obtained for all methods. The running average over the MC trajectories, the corresponding pair correlation functions, and additional computational details are reported in the supplementary material.[172]

The reported average values show the systematic large underestimation of the computed density when dispersion interactions are neglected as well as the (slight) overestimation when these interactions are included via the D3 correction. The Minnesota type functionals are based on various fractions of Hartree-Fock exchange, going from 0.0, 0.27, to 0.54 for M06L-D3, M06-D3, and M062X-D3, respectively. While M062X-D3 performs remarkably well in both reproducing the liquid density (1.004 g/ml) and $g_{OO}(r)$, for the two other functionals, the computed ρ is ~20% too high, and the RDFs lose completely the mid and long range structure. The M06L-D3, M06-D3 can thus not be recommended for the simulation of liquid water. For the considered non-local van der Waals functionals, the obtained results show a larger density of ~8%, and the structure of the liquid is rather well reproduced but with all features shifted to shorter distances. These results are in agreement with previous NVT simulations,[42] and a recent NPT simulation performed with the rVV10 functional in Ref. 74, where a reparameterization of the functional was proposed to cure this deficiency. Even though at the limit of statistical accuracy, both the inclusion of the D3 correction and the use of hybrid functionals reduce the height of the first peak of the $g_{OO}(r)$ for PBE, while the ADMM approximation influences the equilibrium density by ~2% and leads to slightly more

TABLE I. Average density and structural data obtained from the NpT-MC simulations ($T = 295$ K and $p = 1$ bar). ADMM stands for the auxiliary density matrix method[49] that utilizes an auxiliary (smaller) basis to approximate the non-local exchange energy at reduced cost. The methods labeled with optB88-vdW[140,141] and rVV10[71] represent functionals of the non-local van der Waals type. M062X, M06, and M06L are members of the Minnesota type meta-GGA functionals.[142,143] The label D3 stands for the Grimme's type dispersion correction.[68] For PWPB95-D3 only the low density (LD) results are reported. For the calculated average densities, an error estimation has been performed and reported in the table as $\pm\Delta_\rho$. The number of MC cycles for each simulation employed for the calculation of the average properties is reported in the last column, the detailed definition of MC cycle with the computational cost associated to each method together with the corresponding running averages, and pair correlation functions are given in the supplementary material.[172]

	Density (g/ml)		1st max		1st min		2nd max		Simulation length
	ρ	Δ_ρ	r (Å)	$g_{OO}(r)$	r (Å)	$g_{OO}(r)$	r (Å)	$g_{OO}(r)$	(kc)
BLYP	0.797	0.008	2.83	3.04	3.46	0.44	4.65	1.37	41.9
PBE0 (ADMM)	0.832	0.006	2.78	3.28	3.42	0.35	4.53	1.48	30.9
BLYP-D3	1.066	0.007	2.78	2.78	3.51	0.92	4.37	1.11	77.3
PBE-D3	1.055	0.006	2.73	3.07	3.25	0.69	4.43	1.21	41.6
PBE0-D3 (ADMM)	1.023	0.004	2.74	3.13	3.30	0.65	4.52	1.25	30.2
PBE0-D3	1.053	0.005	2.74	2.88	3.29	0.79	4.32	1.21	52.4
M062X-D3 (ADMM)	1.004	0.008	2.78	3.00	3.45	0.78	4.68	1.17	58.6
M06-D3 (ADMM)	1.235	0.003	2.82	2.82	...	...	...	...	21.9
M06L-D3	1.170	0.004	2.82	2.82	...	...	...	...	47.0
optB88-vdW	1.081	0.003	2.74	2.94	3.34	0.80	4.31	1.21	46.8
rVV10	1.078	0.005	2.73	3.22	3.32	0.79	4.40	1.22	41.0
MP2	1.020	0.004	2.76	3.05	3.32	0.72	4.41	1.21	14.6
PWPB95-D3 (LD)	1.002	0.002	2.80	2.80	3.60	0.86	4.59	1.12	17.0
RPA	0.994	0.006	2.78	2.93	3.41	0.78	4.49	1.19	26.8
Exp.	1.00		2.80	2.57	3.45	0.84	4.5	1.12	

structured $g_{OO}(r)$. This combined effect of dispersion and exchange has been emphasized recently.[51] GGA functionals, which underestimate the band gap, lead to a too polarizable solvent, which in turn should lead to too strong hydrogen bonds. This is similar to the effect of charge transfer from anions to the solvent that has been observed to be too strong for GGAs as compared to hybrids.[144] The effect of hybrid functionals on the dielectric constant of water ice has been quantified[45] showing in a quantitative way that GGA functionals lead to more polar structures while also overestimating the polarization of these structures. Whereas the effect of band gap underestimation is already noticeable in neat water, it becomes even more visible in the context of aqueous electrochemistry. Redox levels of various species can be significantly influenced, if water band edges are incorrect, in particular will be pushed up if these are close to the valence band of the liquid.[44] This highlights the importance of going beyond the neat liquid in assessing the performance of electronic structure theory for liquid water.

V. NUCLEAR QUANTUM EFFECTS

The results discussed so far are all based on the assumption that NQEs are small, and that the nuclei can be described classically. In this section, these results are refined by an approximate treatment of NQE based on a QT as proposed in Ref. 132. This quantum thermostat establishes a steady state in the system by enforcing a frequency dependent temperature, which gives a configurational sampling including NQE in the limit of decoupled harmonic modes. The method is an approximation if the coupling between modes is strong, but more accurate than a simple scaling of the temperature in a canonical (NVT) simulation.[51] It is thus an expedient approach with a computational cost that is identical to standard Born-Oppenheimer molecular dynamics. At increased computational cost, it can be combined with path integral (PI) MD, increasing the accuracy of either methods alone. Such results for liquid water were recently presented in Ref. 145. Here, we apply this QT on top of the PBE0-ADMM-D3 functional with a consistent set of simulation parameters. The RDF's obtained for H_2O and D_2O including NQE, as well as the results for classical nuclei, are reported in Figure 3. The positions of the maxima and minima of the $g(r)$ are influenced only

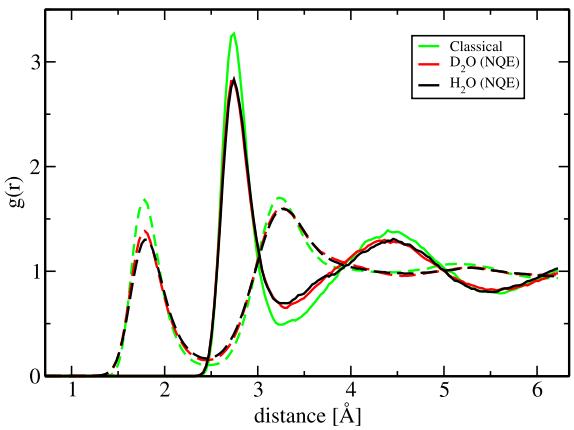

FIG. 3. Oxygen-oxygen (solid lines) and oxygen-hydrogen (dashed lines) radial distribution functions obtained from MD simulations based on the PBE0-ADMM-D3 functional with and without quantum thermostat. Black: H_2O (NQE), red: D_2O (NQE), green: classical nuclei.

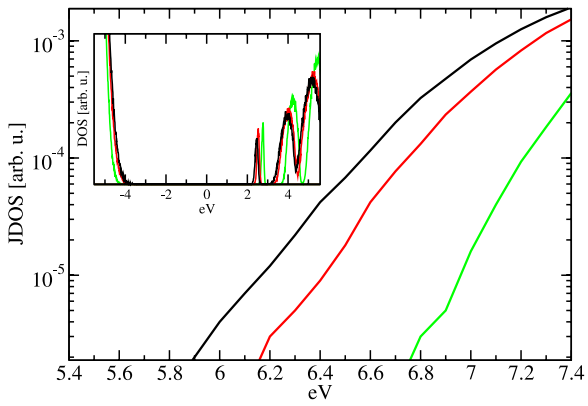

FIG. 4. Shown is the influence of nuclear quantum effects (NQEs) on the electronic structure through a plot of the joint density of state (JDOS) obtained from MD simulations based on the PBE0-ADMM-D3 functional with and without quantum thermostat. Black: H_2O (NQE), red: D_2O (NQE), green: classical nuclei. The inset shows the density of states from which the JDOS has been derived.

marginally. However, NQE leads to a softening of the RDF's and reduces the height of the first peak of the oxygen-oxygen $g(r)$ for both H_2O and D_2O by roughly 10% compared to the classical simulation. Such softening is observed for both *ab initio*[146] and empirical potentials,[21,147–149] but is less pronounced in recent simulations using advanced empirical potentials (Medders *et al.* in Ref. 21). Without further, computationally demanding, path integral simulations, it cannot be excluded that zero-point energy leakage,[150] which might result from the approximations inherent to the QT employed, contributes in part to the observed softening. However, Ceriotti *et al.* have emphasized in Ref. 151 that the competing quantum effects that govern the behavior of water might delicately depend on the functional or potential energy surface. Given the relatively good quality of the PBE0-ADMM-D3 functional, we expect these NQEs to reflect the intrinsic NQE in liquid water, and simulations that do not include NQE must thus display an overstructuring with respect to experiment. Functionals that match the experimental $g(r)$ without considering NQE will thus be understructured in simulations including NQE. A reasonable amount of overstructuring is observed for the $g(r)$ obtained for the MP2 and RPA simulations, and we anticipate that correcting these levels of theory for NQE will result in a near quantitative agreement of these $g(r)$ with the experiments shown. Finally, NQE on the electronic structure of liquid water is found to be important. This result is well known from the field of semi-conductors,[152] but the magnitude is often underestimated. Indeed, accurate experimental results for diamond show a reduction of the band gap on the order of 0.7 eV due to quantum effects.[152] This result has been reproduced by PI MD simulations.[153] Very recently, the broadening of the density of states (DOSs) has been observed in PI MD of (GGA) liquid water, but not analyzed in more detail.[145] To do so, we plot the joint density of states (JDOSs) as shown in Figure 4. The JDOS is the distribution of the energy differences between valence and conduction band eigenstates (HOMO and LUMO orbitals) and can serve as a first (crude) approximation to the optical spectrum. Here, we find that NQE from classical to quantum H_2O shifts the onset of absorption by ∼0.6 eV. The difference between H_2O and D_2O is still ∼0.2 eV, despite their similar O–O $g(r)$. This difference is in agreement with the experimentally observed shift in the ultraviolet absorption edge between H_2O and D_2O, but the estimated shifts depend somewhat on the precise value of the JDOS used for comparison (here 10^{-4}). The computed JDOS onset at the PBE0-ADMM-D3 level of theory matches the onset of absorption at approximately 5.8 eV at 25 °C.[154] Note that also for water ice PBE0 reproduces the experimental bandgap (8.2 vs. 7.8) rather well.[155] The large ∼0.6 eV reduction in band gap induced by NQE is a significant effect and might be observable in the chemistry of aqueous systems. We recommend to take this effect into account if high level electronic structure approaches are to be compared with experiment.[156,157]

VI. DENSITY OF ICE I*h*

As a next step, the densities of liquid water and ice I*h* are compared. The equilibrium parameters calculated at the MP2, PWPB95-D3, and RPA, obtained from the lattice parameter optimization curves of Figure 5, are reported in Table II. At the RPA level, the computed equilibrium molecular volume and cohesive energy compare well with 32.8 Å^3 and −52.5 kJ/mol calculated by Macher *et al.*[159] as well as at the MP2 level the E_{coh} is in good agreement with the value of −58.7 kJ/mol reported by Gillan and coworkers.[160] The results obtained at the PBE level reproduce various previous calculations[74,159,161,162] (see also Table XI in the supplementary material[172]). Note

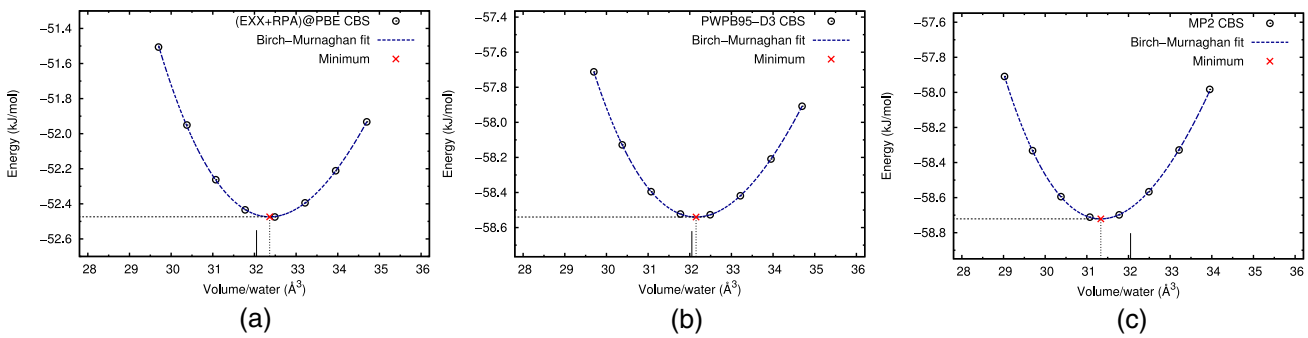

FIG. 5. Cohesive energy per water molecule as a function of the molecular volume for ice I_h evaluated at the (EXX+RPA)@PBE (a), PWPB95-D3 (b), and MP2 (c) level. The correlation energies have been extrapolated to the complete basis set limit and the results have been fitted with a 3rd order Birch-Murnaghan equation of state. In the plot, the minimum obtained from the fitting procedure is reported with a red cross and its coordinates highlighted with dotted line. The experimental volume is reported as a vertical solid line.

TABLE II. Equilibrium volumes and energies (at 0 K) for ice I*h* expressed per molecule. The calculated values are obtained from the minimum of the curves of Figure 5. No corrections for the quantum nature of the nuclei and zero point energies (ZPEs) have been considered. Experimental values are from Refs. 6 and 158.

	E_{coh} (kJ/mol)	V_{mol} (Å^3)	ρ (g/ml)
PBE	−62.8	30.69	0.975
MP2	−58.7	31.34	0.955
PWPB95-D3	−58.5	32.15	0.930
(EEX+RPA)@PBE	−52.5	32.37	0.924
Expt.	−58.9	32.05	0.933

that these results have been obtained 0 K without corrections for the quantum nature of the nuclei and zero point energies (ZPEs). However, these effects have been shown to have small influence on the equilibrium volume of low density phases of ice, and at the PBE level, Santra *et al.*[161] found that the ZPE leads to an increase of the equilibrium volume of ice I*h* by ∼0.5%. Pamuk and coworkers[163] find an increase by less than 1% for the PBE and vdW-DF functionals. Experimentally, these effects have been quantified by comparing the molar volume of ice I*h* for H_2O and D_2O extrapolated to 0 K, showing that the former is only ∼0.1% smaller than the latter.[164,165] Compared to experiment, RPA underestimates the result, but as already pointed out in Ref. 159, this depends on the starting orbitals used. While PBE orbitals lead to underbinding, HF orbitals lead to overbinding, and hybrids can be tuned to yield the correct results. All methods considered yield good results for V_{mol}. Similar to the liquid case, calculated densities are ∼2% larger and ∼1% smaller than experimental results for MP2 and RPA, respectively. These two approaches thus yield the non-trivial prediction that ice floats on water, with a quantitatively correct ratio of liquid and solid density.

VII. DYNAMICAL PROPERTIES

Monte Carlo is a powerful technique to compute ensemble averages, but cannot be used to compute time correlation functions. However, the time evolution of a system relates to several properties that can often be precisely measured experimentally. Two examples that will be discussed in more detail below are the diffusion constant and the infrared spectrum. They can be obtained from the time evolution of the mean square displacement and the Fourier transform of the dipole-dipole correlation function, respectively. If the forces on the ions can be computed, and nuclear quantum effects ignored, Born-Oppenheimer molecular dynamics simulations in the micro-canonical (NVE) ensemble can be employed to generate trajectories and compute dynamical properties. Recently, we have developed the theory and implemented the forces for the RI-GPW-MP2 method,[99] which for the first time allows for a quantitative assessment of the dynamical properties of liquid water at this level of theory. Here, the analysis is based on two trajectories of each roughly 10 ps, obtained in the NVE ensemble, started from equilibrated configurations of earlier MC runs. The length of the simulations is limited by the computational

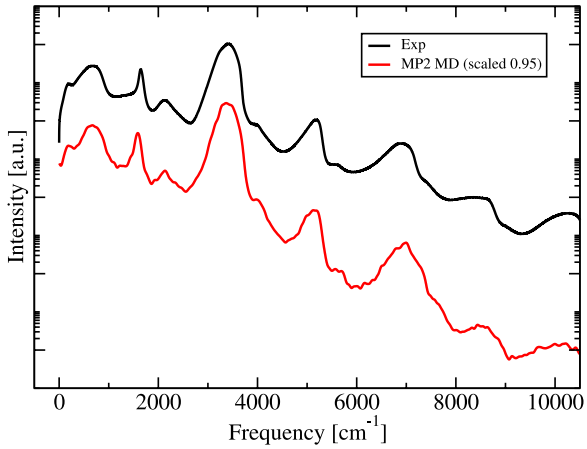

FIG. 6. Shown is a comparison between the experimental (black, Ref. 166) and simulated (red) vibrational spectrum of liquid water, using a logarithmic scale for the intensity to highlight the details of the spectrum between the main peaks and at high frequencies. To facilitate the comparison, the computed spectrum is scaled in frequency by 0.95.

resources required (several millions of core hours), and statistical uncertainty remains non-negligible.

First, the computed and experimental[166] IR spectra of liquid water are compared in Fig. 6. Good agreement over a wide range of frequencies is observed, including the bands at 200 and 2130 cm^{-1}, and various overtones in the range 4000-10 000 cm^{-1}. This provides further support for the suitability of MP2 theory to describe bulk liquid water. It is important to emphasize that the computed data in shown in Fig. 6 have been scaled by 0.95. Without scaling, frequencies are overestimated, as can be expected from a simulation based on Born-Oppenheimer MD, since nuclear quantum effects lower the frequencies. For example, the OH stretch is experimentally at 3409 cm^{-1}, while the computed stretch is at 3563 cm^{-1}. This difference, however, is in agreement with recent estimates of NQE by Paesani and Medders in Ref. 167 (100-150 cm^{-1}) and Fritsch *et al.* in Ref. 149 (220 cm^{-1}), using force fields derived from coupled cluster and density functional theory, respectively. These numbers suggest that this NQE can be expected to depend sensitively on the nature of the potential energy surface. Note that GGA DFT and even hybrids such as PBE0 underestimate the frequency of the OH stretch,[50] leading in the latter case to fortuitous agreement with experiment if corrections for NQE are omitted. Scaling frequencies are only an approximate way to take NQE into account. For example, the optimal multiplication factor is smaller for the bending frequency, where the difference between experiment (1646^{-1}) and MP2 (1669^{-1}) is smaller. Also in this case, the difference is in fair agreement with the estimated NQE by Fritsch *et al.* (44 cm^{-1}).

The second property analyzed is the self-diffusion constant, and the values obtained are 0.67 and 0.77×10^{-5} cm^2/s for simulations at 300 and 307 K, respectively. This is below the value of 2.30×10^{-5} cm^2/s, which is the experimental number at room temperature, and more similar to the value observed at lower temperatures.[168,169] However, such a direct comparison ignores the effect of simulation cell size, NQE, and temperature, which are all important. A more detailed comparison with experiment and various required corrections

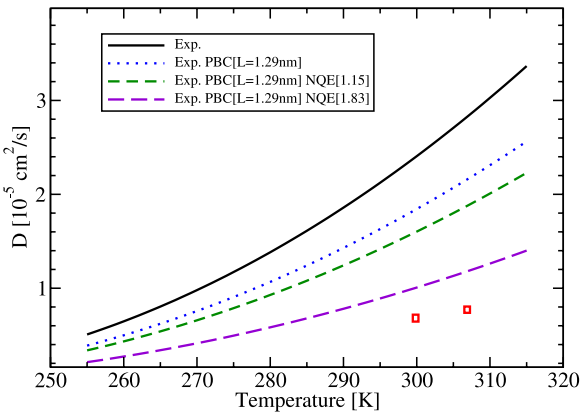

FIG. 7. Shown is the experimental diffusion constant of water as a function of temperature (solid line), as well as the necessary corrections to compare to simulation, namely, a correction for size effects (dotted lines), and in addition for NQE (dashed lines). Simulation results are represented by red squares.

is shown in Fig. 7. First, the diffusion constant obtained in simulation depends quite strongly on the size of the unit cell, being proportional to the viscosity of the liquid and inverse proportional to the length of the edge of the simulation cell.[170] Using the experimental temperature dependent viscosity, an estimate for the diffusion constant of a simulation cell containing 64 water molecules can be obtained (dotted line in Fig. 7). Second, NQE is important also for the diffusion constant, quantum water being more diffusive than classical water by a factor that ranges from 1.15 to 1.83 (dashed lines in Fig. 7), the latter number being most recent and based on an advanced potential model.[21,171] Medders *et al.*[21] have recently emphasized that the effect of NQE for the diffusion constant depends sensitively on the underlying potential energy surface, thus explaining the wide range of values reported in the literature. Comparing MP2 simulation results with the temperature corrected curves, the agreement is good and the error equivalent to an uncertainty in the temperature of approximately 10-20 K.

To summarize, dynamical properties of liquid water have been investigated with MP2 based molecular dynamics simulations, yielding agreement with experiment, after appropriate corrections have been applied. These results suggest that the MP2 potential energy surface of bulk liquid water is of high quality, and that the explicit consideration of nuclear quantum effects in particular might be at least as important as further refinements to the interaction potential.

VIII. CONCLUSIONS

In this work, a series of simulations of bulk liquid water at ambient conditions has been performed, with a focus on methods belonging to the 5th rung of "Jacob's ladder," which include non-local electron correlation. This class of simulations, including the RPA, double-hybrids, and MP2, has been enabled by the RI-GPW method and its high performance implementation.[99,111,115] These simulations demonstrate that MP2 and RPA, which treat hydrogen bonding and van der Waals interactions at equal footing, provide a density of water that is in good agreement with experiment. Indeed, a variety of methods including dispersion in a less seamless way lead to densities that are too high, while plain GGA methods lead to too low densities, consistent with these approaches favoring different phases (LDL and HDL) of water. The double hybrid approach PWPB95-D3 initially provided good results but leads to a too high density after longer simulation. MP2 and RPA both predict that ice floats on water, with a quantitatively correct estimate of their density ratio, contrary to most other approaches. The detailed structure of MP2 and RPA, as characterized by the $g_{OO}(r)$, is in good agreement with experiment with a slightly overstructured $g_{OO}(r)$. Nuclear quantum effects are expected to reduce the first peak of the $g_{OO}(r)$ by roughly 10%, which would result in excellent agreement with experiment. We furthermore find an important NQE (0.6 eV) on the band gap of liquid water, with a 0.2 eV H_2O–D_2O shift in the JDOS that is in excellent agreement with experimental optical absorption spectra. With the availability of MP2 gradients, time correlation functions can be computed at this level of theory. These reveal that the IR spectrum, over a wide range of frequencies including overtones, and the diffusion constant are in good agreement with experiment, but only after NQEs have been taken into account. This establishes incorporating NQEs in electronic structure based simulations as a key factor for reaching quantitative agreement with experimental data on liquid water, possibly more important than further refinements to the potential energy surface. The simulations presented here demonstrate the feasibility and quality of RPA and MP2 for the simulation of bulk liquid water, and strongly suggest the application of these methods as high quality reference methods for a wide range of applications in aqueous chemistry and physics.

ACKNOWLEDGMENTS

The authors thank Claudia Draxl for bringing the importance of NQE in Diamond (Ref. 152) to our attention, and Gustavo Scuseria and Georg Kresse for computing benchmark M06L reference data on condensed phase structures that validated our implementation. J.V. acknowledges financial support by the European Union FP7 in the form of an ERC Starting Grant under Contract No. 277910. This research was partly supported by NCCR MARVEL, funded by the Swiss National Science Foundation. We acknowledge that the results of this research have been achieved using the PRACE Research Infrastructure resource Hermit based in Germany at Stuttgart (HLRS). Additional calculations were enabled by the Swiss National Supercomputer Centre (CSCS) under project ID ch5. The research leading to these results has received funding from the Swiss University Conference through the High Performance and High Productivity Computing (HP2C) Programme.

[1]J. R. Errington and P. G. Debenedetti, Nature **409**, 318 (2001).
[2]P. Wernet, D. Nordlund, U. Bergmann, M. Cavalleri, M. Odelius, H. Ogasawara, L. A. Näslund, T. K. Hirsch, L. Ojamäe, P. Glatzel, L. G. M. Pettersson, and A. Nilsson, Science **304**, 995 (2004).
[3]A. K. Soper, ISRN Phys. Chem. **2013**, 279463 (2013).
[4]A. Nilsson and L. Pettersson, Chem. Phys. **389**, 1 (2011).
[5]A. Rahman and F. H. Stillinger, J. Chem. Phys. **55**, 3336 (1971).
[6]E. Whalley, J. Chem. Phys. **81**, 4087 (1984).
[7]G. A. Tribello and B. Slater, Chem. Phys. Lett. **425**, 246 (2006).
[8]W. L. Jorgensen, J. Chandrasekhar, J. D. Madura, R. W. Impey, and M. L. Klein, J. Chem. Phys. **79**, 926 (1983).

[9]B. Guillot, J. Mol. Liq. **101**, 219 (2002).
[10]W. L. Jorgensen and J. Tirado-Rives, Proc. Natl. Acad. Sci. U. S. A. **102**, 6665 (2005).
[11]R. Bukowski, K. Szalewicz, G. C. Groenenboom, and A. van der Avoird, Science **315**, 1249 (2007).
[12]A. G. Donchev, N. G. Galkin, A. A. Illarionov, O. V. Khoruzhii, M. A. Olevanov, V. D. Ozrin, M. V. Subbotin, and V. I. Tarasov, Proc. Natl. Acad. Sci. U. S. A. **103**, 8613 (2006).
[13]M. W. Mahoney and W. L. Jorgensen, J. Chem. Phys. **112**, 8910 (2000).
[14]S. W. Rick, S. J. Stuart, and B. J. Berne, J. Chem. Phys. **101**, 6141 (1994).
[15]S. Izvekov, M. Parrinello, C. J. Burnham, and G. A. Voth, J. Chem. Phys. **120**, 10896 (2004).
[16]S. S. Xantheas, C. J. Burnham, and R. J. Harrison, J. Chem. Phys. **116**, 1493 (2002).
[17]P. Paricaud, M. Predota, A. A. Chialvo, and P. T. Cummings, J. Chem. Phys. **122**, 244511 (2005).
[18]B. Chen, J. Xing, and J. I. Siepmann, J. Phys. Chem. B **104**, 2391 (2000).
[19]T. M. Truskett and K. A. Dill, J. Phys. Chem. B **106**, 11829 (2002).
[20]A. Wallqvist and R. D. Mountain, Rev. Comput. Chem. **13**, 183 (1999).
[21]G. R. Medders, V. Babin, and F. Paesani, J. Chem. Theory Comput. **10**, 2906 (2014).
[22]R. Kumar, F.-F. Wang, G. R. Jenness, and K. D. Jordan, J. Chem. Phys. **132**, 014309 (2010).
[23]P. Hohenberg and W. Kohn, Phys. Rev. **136**, B864 (1964).
[24]W. Kohn and L. J. Sham, Phys. Rev. **140**, A1133 (1965).
[25]K. Laasonen, M. Sprik, M. Parrinello, and R. Car, J. Chem. Phys. **99**, 9080 (1993).
[26]P. L. Silvestrelli and M. Parrinello, J. Chem. Phys. **111**, 3572 (1999).
[27]S. Izvekov and G. A. Voth, J. Chem. Phys. **116**, 10372 (2002).
[28]J. C. Grossman, E. Schwegler, E. W. Draeger, F. Gygi, and G. Galli, J. Chem. Phys. **120**, 300 (2004).
[29]T. D. Kühne, M. Krack, and M. Parrinello, J. Chem. Theory Comput. **5**, 235 (2009).
[30]I.-C. Lin, A. P. Seitsonen, I. Tavernelli, and U. Rothlisberger, J. Chem. Theory Comput. **8**, 3902 (2012).
[31]D. Asthagiri, L. Pratt, and J. Kress, Phys. Rev. E **68**, 041505 (2003).
[32]E. Schwegler, J. C. Grossman, F. Gygi, and G. Galli, J. Chem. Phys. **121**, 5400 (2004).
[33]P. H.-L. Sit and N. Marzari, J. Chem. Phys. **122**, 204510 (2005).
[34]R. Jonchiere, A. P. Seitsonen, G. Ferlat, A. M. Saitta, and R. Vuilleumier, J. Chem. Phys. **135**, 154503 (2011).
[35]J. VandeVondele, F. Mohamed, M. Krack, J. Hutter, M. Sprik, and M. Parrinello, J. Chem. Phys. **122**, 014515 (2005).
[36]H.-S. Lee and M. E. Tuckerman, J. Chem. Phys. **125**, 154507 (2006).
[37]H.-S. Lee and M. E. Tuckerman, J. Chem. Phys. **126**, 164501 (2007).
[38]Z. Ma, Y. Zhang, and M. E. Tuckerman, J. Chem. Phys. **137**, 044506 (2012).
[39]M. V. Fernández-Serra and E. Artacho, J. Chem. Phys. **121**, 11136 (2004).
[40]J. Schmidt, J. VandeVondele, I.-F. W. Kuo, D. Sebastiani, J. I. Siepmann, J. Hutter, and C. J. Mundy, J. Phys. Chem. B **113**, 11959 (2009).
[41]M. J. McGrath, J. I. Siepmann, I.-F. W. Kuo, C. J. Mundy, J. VandeVondele, J. Hutter, F. Mohamed, and M. Krack, ChemPhysChem **6**, 1894 (2005).
[42]J. Wang, G. Román-Pérez, J. M. Soler, E. Artacho, and M.-V. Fernández-Serra, J. Chem. Phys. **134**, 024516 (2011).
[43]M. Del Ben, M. Schönherr, J. Hutter, and J. VandeVondele, J. Phys. Chem. Lett. **4**, 3753 (2013).
[44]C. Adriaanse, J. Cheng, V. Chau, M. Sulpizi, J. VandeVondele, and M. Sprik, J. Phys. Chem. Lett. **3**, 3411 (2012).
[45]M. Schoenherr, B. Slater, J. Hutter, and J. VandeVondele, J. Phys. Chem. B **118**, 590 (2014).
[46]J. P. Perdew, A. Ruzsinszky, J. Tao, V. N. Staroverov, G. E. Scuseria, and G. I. Csonka, J. Chem. Phys. **123**, 062201 (2005).
[47]T. Todorova, A. Seitsonen, J. Hutter, I. Kuo, and C. Mundy, J. Phys. Chem. B **110**, 3685 (2006).
[48]M. Guidon, F. Schiffmann, J. Hutter, and J. VandeVondele, J. Chem. Phys. **128**, 214104 (2008).
[49]M. Guidon, J. Hutter, and J. VandeVondele, J. Chem. Theory Comput. **6**, 2348 (2010).
[50]C. Zhang, D. Donadio, F. Gygi, and G. Galli, J. Chem. Theory Comput. **7**, 1443 (2011).
[51]R. A. DiStasio, B. Santra, Z. Li, X. Wu, and R. Car, J. Chem. Phys. **141**, 084502 (2014).
[52]D. C. Langreth and J. P. Perdew, Phys. Rev. B **15**, 2884 (1977).
[53]D. Langreth and J. Perdew, Solid State Commun. **17**, 1425 (1975).
[54]O. Gunnarsson and B. I. Lundqvist, Phys. Rev. B **13**, 4274 (1976).
[55]M. Fuchs and X. Gonze, Phys. Rev. B **65**, 235109 (2002).
[56]F. Furche and T. V. Voorhis, J. Chem. Phys. **122**, 164106 (2005).
[57]A. Heßelmann and A. Görling, Mol. Phys. **109**, 2473 (2011).
[58]H. Eshuis, J. Bates, and F. Furche, Theor. Chem. Acc. **131**, 1084 (2012).
[59]J. Paier, X. Ren, P. Rinke, G. E. Scuseria, A. Grüneis, G. Kresse, and M. Scheffler, New J. Phys. **14**, 043002 (2012).
[60]X. Ren, P. Rinke, C. Joas, and M. Scheffler, J. Mater. Sci. **47**, 7447 (2012).
[61]C. Møller and M. S. Plesset, Phys. Rev. **46**, 618 (1934).
[62]A. Szabo and N. S. Ostlund, *Modern Quantum Chemistry* (McGraw Hill, New York, 1982).
[63]A. Görling and M. Levy, Phys. Rev. B **47**, 13105 (1993).
[64]R. J. Bartlett, I. Grabowski, S. Hirata, and S. Ivanov, J. Chem. Phys. **122**, 034104 (2005).
[65]S. Grimme, J. Chem. Phys. **124**, 034108 (2006).
[66]T. Schwabe and S. Grimme, Phys. Chem. Chem. Phys. **8**, 4398 (2006).
[67]L. Goerigk and S. Grimme, J. Chem. Theory Comput. **7**, 291 (2011).
[68]S. Grimme, J. Antony, S. Ehrlich, and H. Krieg, J. Chem. Phys. **132**, 154104 (2010).
[69]M. Dion, H. Rydberg, E. Schröder, D. C. Langreth, and B. I. Lundqvist, Phys. Rev. Lett. **92**, 246401 (2004).
[70]M. Dion, H. Rydberg, E. Schröder, D. C. Langreth, and B. I. Lundqvist, Phys. Rev. Lett. **95**, 109902 (2005).
[71]R. Sabatini, T. Gorni, and S. de Gironcoli, Phys. Rev. B **87**, 041108 (2013).
[72]O. A. Vydrov and T. Van Voorhis, J. Chem. Phys. **133**, 244103 (2010).
[73]A. Bankura, A. Karmakar, V. Carnevale, A. Chandra, and M. L. Klein, J. Phys. Chem. C **118**, 29401 (2014).
[74]G. Miceli, S. de Gironcoli, and A. Pasquarello, J. Chem. Phys. **142**, 034501 (2015).
[75]I.-F. W. Kuo, C. J. Mundy, M. J. McGrath, J. I. Siepmann, J. VandeVondele, M. Sprik, J. Hutter, B. Chen, M. L. Klein, F. Mohamed, M. Krack, and M. Parrinello, J. Phys. Chem. B **108**, 12990 (2004).
[76]M. J. McGrath, J. I. Siepmann, I.-F. W. Kuo, and C. J. Mundy, Mol. Phys. **104**, 3619 (2006).
[77]R. Iftimie, D. Salahub, D. Wei, and J. Schofield, J. Chem. Phys. **113**, 4852 (2000).
[78]B. Hetenyi, K. Bernacki, and B. J. Berne, J. Chem. Phys. **117**, 8203 (2002).
[79]L. D. Gelb, J. Chem. Phys. **118**, 7747 (2003).
[80]S. Duane, A. Kennedy, B. J. Pendleton, and D. Roweth, Phys. Lett. B **195**, 216 (1987).
[81]B. Mehlig, D. W. Heermann, and B. M. Forrest, Phys. Rev. B **45**, 679 (1992).
[82]M. Del Ben, M. Schönherr, J. Hutter, and J. VandeVondele, J. Phys. Chem. Lett. **5**, 3066 (2014).
[83]S. Hirata, X. He, M. R. Hermes, and S. Y. Willow, J. Phys. Chem. A **118**, 655 (2014).
[84]S. Saebø and P. Pulay, Annu. Rev. Phys. Chem. **44**, 213 (1993).
[85]P. Pulay and S. Saebø, Theor. Chim. Acta **69**, 357 (1986).
[86]G. Rauhut, P. Pulay, and H.-J. Werner, J. Comput. Chem. **19**, 1241 (1998).
[87]M. Schütz, G. Hetzer, and H.-J. Werner, J. Chem. Phys. **111**, 5691 (1999).
[88]G. Hetzer, M. Schütz, H. Stoll, and H.-J. Werner, J. Chem. Phys. **113**, 9443 (2000).
[89]S. Saebø and P. Pulay, J. Chem. Phys. **115**, 3975 (2001).
[90]C. Pisani, M. Busso, G. Capecchi, S. Casassa, R. Dovesi, L. Maschio, C. Zicovich-Wilson, and M. Schütz, J. Chem. Phys. **122**, 094113 (2005).
[91]C. Pisani, L. Maschio, S. Casassa, M. Halo, M. Schütz, and D. Usvyat, J. Comput. Chem. **29**, 2113 (2008).
[92]P. Maslen, Chem. Phys. Lett. **283**, 102 (1998).
[93]P. E. Maslen and M. Head-Gordon, J. Chem. Phys. **109**, 7093 (1998).
[94]J. L. Whitten, J. Chem. Phys. **58**, 4496 (1973).
[95]B. I. Dunlap, J. W. D. Connolly, and J. R. Sabin, J. Chem. Phys. **71**, 3396 (1979).
[96]O. Vahtras, J. Almlöf, and M. Feyereisen, Chem. Phys. Lett. **213**, 514 (1993).
[97]M. Feyereisen, G. Fitzgerald, and A. Komornicki, Chem. Phys. Lett. **208**, 359 (1993).
[98]W. Klopper, F. R. Manby, S. Ten-No, and E. F. Valeev, Int. Rev. Phys. Chem. **25**, 427 (2006).
[99]M. Del Ben, J. Hutter, and J. VandeVondele, J. Chem. Phys. **143**, 102803 (2015).
[100]F. Weigend and M. Häser, Theor. Chem. Acc. **97**, 331 (1997).
[101]R. A. Distasio, R. P. Steele, Y. M. Rhee, Y. Shao, and M. Head-Gordon, J. Comput. Chem. **28**, 839 (2007).
[102]C. Hättig, A. Hellweg, and A. Köhn, Phys. Chem. Chem. Phys. **8**, 1159 (2006).
[103]C. M. Aikens, S. P. Webb, R. L. Bell, G. D. Fletcher, M. W. Schmidt, and M. S. Gordon, Theor. Chem. Acc. **110**, 233 (2003).

[104]J. P. Perdew, J. A. Chevary, S. H. Vosko, K. A. Jackson, M. R. Pederson, D. J. Singh, and C. Fiolhais, Phys. Rev. B **46**, 6671 (1992).
[105]J. P. Perdew, J. A. Chevary, S. H. Vosko, K. A. Jackson, M. R. Pederson, D. J. Singh, and C. Fiolhais, Phys. Rev. B **48**, 4978 (1993).
[106]A. D. Becke, J. Chem. Phys. **104**, 1040 (1996).
[107]S. Grimme, J. Chem. Phys. **118**, 9095 (2003).
[108]Y. Jung, R. C. Lochan, A. D. Dutoi, and M. Head-Gordon, J. Chem. Phys. **121**, 9793 (2004).
[109]J. Almlöf, Chem. Phys. Lett. **181**, 319 (1991).
[110]M. Häser and J. Almlöf, J. Chem. Phys. **96**, 489 (1992).
[111]M. Del Ben, J. Hutter, and J. VandeVondele, J. Chem. Theory Comput. **9**, 2654 (2013).
[112]F. Furche, Phys. Rev. B **64**, 195120 (2001).
[113]H. Eshuis, J. Yarkony, and F. Furche, J. Chem. Phys. **132**, 234114 (2010).
[114]A. Takatsuka, S. Ten-no, and W. Hackbusch, J. Chem. Phys. **129**, 044112 (2008).
[115]M. Del Ben, O. Schütt, T. Wentz, P. Messmer, J. Hutter, and J. VandeVondele, Comput. Phys. Commun. **187**, 120 (2015).
[116]See http://www.cp2k.org/ for the CP2K developers group, 2014.
[117]G. Lippert, J. Hutter, and M. Parrinello, Mol. Phys. **92**, 477 (1997).
[118]J. VandeVondele, M. Krack, F. Mohamed, M. Parrinello, T. Chassaing, and J. Hutter, Comput. Phys. Commun. **167**, 103 (2005).
[119]T. H. Dunning, J. Chem. Phys. **90**, 1007 (1989).
[120]D. E. Woon and T. H. Dunning, J. Chem. Phys. **98**, 1358 (1993).
[121]M. Del Ben, J. Hutter, and J. VandeVondele, J. Chem. Theory Comput. **8**, 4177 (2012).
[122]S. Goedecker, M. Teter, and J. Hutter, Phys. Rev. B **54**, 1703 (1996).
[123]M. Guidon, J. Hutter, and J. VandeVondele, J. Chem. Theory Comput. **5**, 3010 (2009).
[124]J. P. Perdew, K. Burke, and M. Ernzerhof, Phys. Rev. Lett. **77**, 3865 (1996).
[125]A. D. Becke, Phys. Rev. A **38**, 3098 (1988).
[126]C. Lee, W. Yang, and R. G. Parr, Phys. Rev. B **37**, 785 (1988).
[127]E. E. Dahlke and D. G. Truhlar, J. Phys. Chem. B **109**, 15677 (2005).
[128]C. Adamo and V. Barone, J. Chem. Phys. **110**, 6158 (1999).
[129]A. Halkier, T. Helgaker, P. Jørgensen, W. Klopper, H. Koch, J. Olsen, and A. K. Wilson, Chem. Phys. Lett. **286**, 243 (1998).
[130]H. Eshuis and F. Furche, J. Chem. Phys. **136**, 084105 (2012).
[131]R. Ramírez, T. López-Ciudad, P. P. Kumar, and D. Marx, J. Chem. Phys. **121**, 3973 (2004).
[132]M. Ceriotti, G. Bussi, and M. Parrinello, Phys. Rev. Lett. **103**, 030603 (2009).
[133]M. Ceriotti, G. Bussi, and M. Parrinello, J. Chem. Theory Comput. **6**, 1170 (2010).
[134]L. B. Skinner, C. Huang, D. Schlesinger, L. G. M. Pettersson, A. Nilsson, and C. J. Benmore, J. Chem. Phys. **138**, 074506 (2013).
[135]T. D. Kühne, T. A. Pascal, E. Kaxiras, and Y. Jung, J. Phys. Chem. Lett. **2**, 105 (2011).
[136]F. Corsetti, E. Artacho, J. M. Soler, S. S. Alexandre, and M.-V. Fernández-Serra, J. Chem. Phys. **139**, 194502 (2013).
[137]L. G. Pettersson and A. Nilsson, J. Non-Cryst. Solids **407**, 399 (2014).
[138]P. Jurecka, J. Sponer, J. Cerny, and P. Hobza, Phys. Chem. Chem. Phys. **8**, 1985 (2006).
[139]T. Takatani, E. G. Hohenstein, M. Malagoli, M. S. Marshall, and C. D. Sherrill, J. Chem. Phys. **132**, 144104 (2010).
[140]J. Klimeš, D. Bowler, and A. Michaelides, J. Phys.: Condens. Matter **22**, 022201 (2010).
[141]J. Klimeš, D. Bowler, and A. Michaelides, Phys. Rev. B **83**, 1 (2011).
[142]Y. Zhao and D. G. Truhlar, J. Chem. Phys. **125**, 194101 (2006).
[143]Y. Zhao and D. G. Truhlar, Theor. Chem. Acc. **120**, 215 (2007).
[144]J. VandeVondele, P. Troester, P. Tavan, and G. Mathias, J. Phys. Chem. A **116**, 2466 (2012).
[145]F. Giberti, A. A. Hassanali, M. Ceriotti, and M. Parrinello, J. Phys. Chem. B **118**, 13226 (2014).
[146]J. A. Morrone and R. Car, Phys. Rev. Lett. **101**, 017801 (2008).
[147]F. Paesani, S. Iuchi, and G. A. Voth, J. Chem. Phys. **127**, 074506 (2007).
[148]G. S. Fanourgakis, G. K. Schenter, and S. S. Xantheas, J. Chem. Phys. **125**, 141102 (2006).
[149]S. Fritsch, R. Potestio, D. Donadio, and K. Kremer, J. Chem. Theory Comput. **10**, 816 (2014).
[150]S. Habershon and D. E. Manolopoulos, J. Chem. Phys. **131**, 244518 (2009).
[151]M. Ceriotti and D. E. Manolopoulos, Phys. Rev. Lett. **109**, 100604 (2012).
[152]M. Cardona and M. L. W. Thewalt, Rev. Mod. Phys. **77**, 1173 (2005).
[153]R. Ramírez, C. P. Herrero, and E. R. Hernández, Phys. Rev. B **73**, 245202 (2006).
[154]T. W. Marin, K. Takahashi, and D. M. Bartels, J. Chem. Phys. **125**, 104314 (2006).
[155]F. Labat, C. Pouchan, C. Adamo, and G. E. Scuseria, J. Comput. Chem. **32**, 2177 (2011).
[156]C. Fang, W.-F. Li, R. S. Koster, J. Klimes, A. van Blaaderen, and M. A. van Huis, Phys. Chem. Chem. Phys. **17**, 365 (2015).
[157]T. A. Pham, C. Zhang, E. Schwegler, and G. Galli, Phys. Rev. B **89**, 060202(R) (2014).
[158]P. Hobbs, *Ice Physics* (Clarendon Press, 1974).
[159]M. Macher, J. Klimes, C. Franchini, and G. Kresse, J. Chem. Phys. **140**, 084502 (2014).
[160]M. J. Gillan, D. Alfè, P. J. Bygrave, C. R. Taylor, and F. R. Manby, J. Chem. Phys. **139**, 114101 (2013).
[161]B. Santra, J. Klimeš, A. Tkatchenko, D. Alfè, B. Slater, A. Michaelides, R. Car, and M. Scheffler, J. Chem. Phys. **139**, 154702 (2013).
[162]P. J. Feibelman, Phys. Chem. Chem. Phys. **10**, 4688 (2008).
[163]B. Pamuk, J. M. Soler, R. Ramírez, C. P. Herrero, P. W. Stephens, P. B. Allen, and M.-V. Fernández-Serra, Phys. Rev. Lett. **108**, 193003 (2012).
[164]K. Röttger, A. Endriss, J. Ihringer, S. Doyle, and W. F. Kuhs, Acta Crystallogr., Sect. B: Struct. Sci. **50**, 644 (1994).
[165]K. Röttger, A. Endriss, J. Ihringer, S. Doyle, and W. F. Kuhs, Acta Crystallogr., Sect. B: Struct. Sci. **68**, 91 (2012).
[166]J. E. Bertie and Z. Lan, Appl. Spectrosc. **50**, 1047 (1996).
[167]G. R. Medders and F. Paesani, J. Chem. Theory Comput. **11**, 1145 (2015).
[168]M. Holz, S. Heil, and A. Sacco, Phys. Chem. Chem. Phys. **2**, 4740 (2000).
[169]W. Price, H. Ide, and Y. Arata, J. Phys. Chem. A **103**, 448 (1999).
[170]I. Yeh and G. Hummer, J. Phys. Chem. B **108**, 15873 (2004).
[171]S. Habershon, T. E. Markland, and D. E. Manolopoulos, J. Chem. Phys. **131**, 024501 (2009).
[172]See supplementary material at http://dx.doi.org/10.1063/1.4927325 for supporting information which includes running averages of the density for 14 different functionals, the corresponding O–O and O–H radial distribution functions, covergence tests of the radial distribution functions with respect to plane wave cutoff for BLYP and M06L, basis set convergence tests, k-point sampling tests, validation of the PBE and M06L energies with respect to pseudopotential and implementation, a comparison of MC and MD sampling, validation of the PWPB95-D3 implementation, detailed computational parameters, including basis sets, pseudopotentials, and various sample input files.